Computation of stress intensity factors in an initiating RCF crack using a 3D modelling approach

Naeimi, Meysam; Li, Zili; Dollevoet, Rolf

Publication date
2017

Document Version
Final published version

Published in
Proceedings of the First International Conference on Rail Transportation

Citation (APA)
Naeimi, M., Li, Z., & Dollevoet, R. (2017). Computation of stress intensity factors in an initiating RCF crack using a 3D modelling approach. In *Proceedings of the First International Conference on Rail Transportation: ICRT2017 , Chengdu, China, July 10-12, 2017*

Important note
To cite this publication, please use the final published version (if applicable).
Please check the document version above.

First International Conference on Rail Transportation
Chengdu, China, July 10-12, 2017

Computation of stress intensity factors in an initiating RCF crack using a 3D modelling approach

Meysam Naeimi[1*], Zili Li[1] and Rolf Dollevoet[1]
[1.] *Section of Railway Engineering, Faculty of Civil Engineering and Geoscience, Delft University of Technology, Delft, the Netherlands*
**Corresponding author email: m.naeimi@tudelft.nl*

Abstract: This research investigates the development process of initiating rolling contact fatigue (RCF) cracks in the rail using a 3D modelling approach. The analysis is based on the application of stress analysis and fracture mechanics. The finite element method is used to describe the crack tip stress environment and to determine the stress intensity factors (SIF) around the crack tip. Dynamic behaviours of the wheel-rail contact are taken into account by including the vehicle-track components in the modelling. A mixed-mode fatigue crack growth is considered. The dominant modes of the crack propagation in a RCF crack at its early stage of development have been calculated. The results of the numerical predictions are compared with those of a benchmark model in the literature. Using these results, the validity of the new modelling approach for calculating SIF is examined.
Keywords: Crack, propagation, rolling contact fatigue, stress intensity factors, finite element model

1 Introduction

Rolling contact fatigue occurs in rail material due to the repetitive passage of wheels on rails under impact loading conditions. When the fatigue crack is initiated in rail, prediction of the crack propagation is important for estimating the crack growth and the rail lifetime. This can prevent the possible fracture of rail by applying in-time maintenance strategies. Corrugations, head checks and squats are examples of RCF defects happening in rail material. A squat appears on rail with a kind of surface depression with general appearance of a two-lung shape damage at their mature status. Rail squats are dangerous defects that can develop into the rail fracture, if they are not treated well and on time. Fig. 1 shows an example of a rail squat from a site in the Netherlands, in which the crack is relatively at its middle phase of development. Squats can also be found with younger cracks than the one shown in this figure; however younger cracks are difficult to distinguish with the naked eyes.

Until now, a considerable amount of research was carried out on the rail fracture analysis and RCF prediction. Calculation of stress intensity factors (SIF) and investigations of fatigue crack growth have been importance phenomena in rail fatigue design for many years. It predicts the stress state near the crack tip caused by loading and residual stresses. It is a useful criterion for providing information on damage development speed and directions of the crack propagation.

Considering the two-dimensional (2D) modelling approaches, see e.g. (Kim and Kim 2002, Ringsberg and Bergkvist 2003), the behaviour of rail RCF cracks were investigated through finite element (FE) stress analysis and fracture mechanics. In these studies, the evolution of stress histories was studied and SIFs are calculated to investigate the fatigue crack propagation process in rail.

Since RCF cracks in rails have a complex 3D crack network, 2D models cannot provide a full understanding on their propagation process. Furthermore, the complex mechanism of the wheel-rail contact and loading conditions cannot be realistically simulated using the 2D models. Therefore, the three-dimensional (3D) models of rail fatigue behaviour were developed to study the development of RCF cracks in 3D; see e.g.

(Bogdanski, Olzak et al. 1998, Bogdański and Lewicki 2008). These models treated the RCF cracks with numerical simulations using finite element method and fracture mechanics. Among these researches, the FE model of (Bogdanski, Olzak et al. 1998) was specifically applied on the squat-type cracks, to predict the crack development mechanism with addressing the shapes, directions of extension and the forms of spalling and branching.

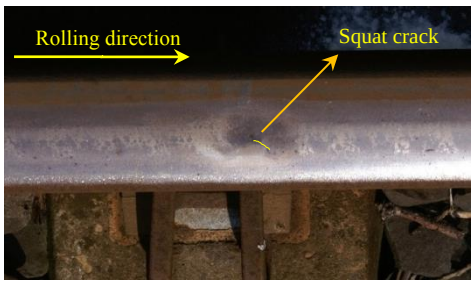

Fig. 1. An example of squat with a crack at its middle stage of development

Although the 3D models can more realistically simulate the loading conditions of the wheel-rail contact problem, they introduced many simplifications. In the aforementioned references, the contact load between wheel and rail has been simplified with elliptical pressure distribution, obtained from the theoretical Hertz solution. Such models also neglected the dynamic interaction of the wheel-track system or at most applied dynamic amplification factors over the static loads. Hence, there still remains a lack of the modelling technique appropriate for dealing with the dynamic contact problem.

This paper seeks to treat this problem by introducing a 3D modelling approach, taking the major components of the wheel-track system into account. The numerical model of the current research deals with transient FE simulations, considering the system dynamic and the contact mechanics. The explicit scheme of the FE analysis allows for investigating the transient rolling contact under high frequency vibrations in the system, a problem which has not received enough attention in the past.

2 Initiating RCF crack

According to (Ringsberg, Loo-Morrey et al. 2000, Ringsberg and Josefson 2001, Pal, Daniel et al. 2013, Simon, Saulot et al. 2013), a squat is generally initiated at the rail surface (or very close to surface) and it grows parallel (or with a shallow angle) to the surface at its early stage of development. Various phases for the shape development in a squat crack are introduced in (Bogdański 2005, Bogdański and Lewicki 2008) based on the observations on a majority of squat defects. Using these works, a semi-elliptical crack, shown in Fig. 2, can be considered as the early stage of RCF crack development in the railhead. This crack is considered as the initiating RCF crack in the present study to target its further development. The geometry of this crack is a half ellipse with oblique angles relative to the XY, XZ and YZ planes. The crack opening is assumed to intersect the rail surface with a straight line skewed with respect to the X direction. The crack plane is supposed to be flat, which means all the nodes on this plane belongs to the prescribed semi-ellipse.

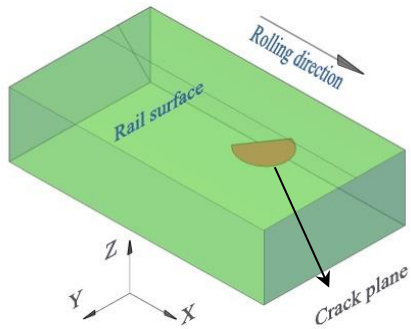

Fig. 2. The initiating RCF crack assumed in the research to target its further development; X, Y and Z are the conventional coordinate system used in the analysis

2.1 Shape, orientation, and dimensions

The geometry of the initiating RCF crack in this research is shown in Fig. 3, where the semi-elliptical crack is illustrated in various 2D planes. The figure shows the orientation and dimensions of the crack in the Cartesian coordinate system. In the figure, c and d are the semi-major axes of the crack; X, Y, Z are the axes of the global coordinate system and θ, φ, ψ are the angles of crack plane in the XZ, XY and YZ planes, respectively. The rail gauge-corner side and the direction of the wheel travel are also shown. Details of the geometrical parameters and crack specifications are given in Table 1.

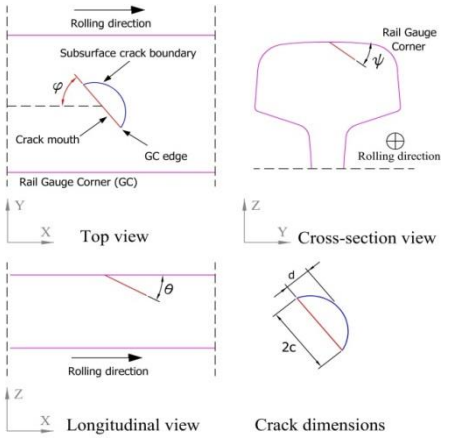

Fig. 3. The shape, orientation, and dimension of squat crack in railhead.

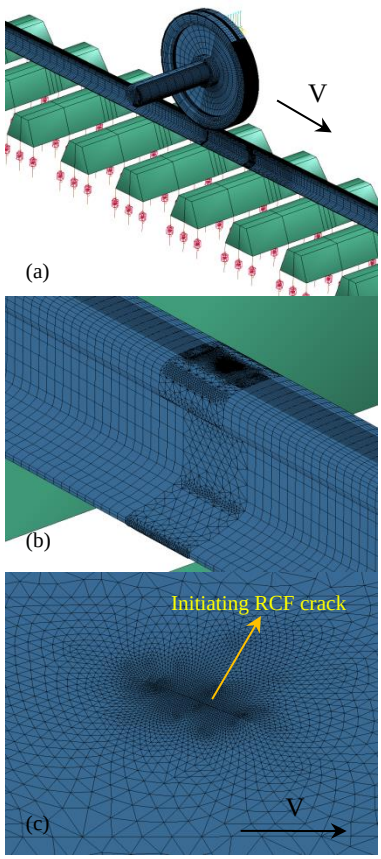

Fig. 4. The FE model of the wheel–track system with implanted RCF crack, (a) overall view, (b) the magnified view of the solution zone, (c) magnification on the RCF crack

Table 1. The assumed geometry of the initiating RCF crack, the wheel and rail dimensions and the size of the contact patch

Parameters	**Values**
Wheel diameter *(mm)*	920
Radius of 54E1 rail profile in lateral plane *(mm)*	300
Semi-major axis of the crack, *c (mm)*	4.30
Semi-minor axis of the crack *d (mm)*	3.00
Semi-major axis of contact patch, calculated by results of FEM, *b (mm)*	7.58
Semi-minor axis of contact patch, calculated by results of FEM, *a (mm)*	5.56
Crack mouth thickness (mm)	0.10
Crack initial angle*, θ	20
Crack initial angle*, φ	45
Crack initial angle*, ψ	20

* A finite element method for calculating initiation angles is presented in (Naeimi, Li et al. 2015)

3 Numerical modelling process

A wide range of finite element models have been introduced for the wheel–rail contact problem over the past years. In most of the works, two solid rolling bodies were put together to generate the rolling contact behaviour. The wheel–rail contact problem with considering vehicle–track interaction was treated in (Zhao and Li 2011, Zhao, Li et al. 2013, Zhao, Li et al. 2014) using an explicit FE method. In this research, the same FE methodology is further developed to be applicable for the rail with RCF crack. A semi-elliptical RCF crack is implanted in the railhead. This model is shown in Fig. 4(a) with magnifications over the RCF crack region in Fig. 4(b, c). The model considers high frequency dynamic behaviours of the wheel–track system excited by the wheel rolling over the rail and associated wave propagations. To reach a sufficient accuracy in FE simulations, the contact zone of the wheel and rail is densely meshed with fine elements. A finer mesh scheme is used in the solution zone with the finest elements of 0.25 mm in the crack area. The mechanical and loading parameters of the wheel-track system are listed in Table 2. Note that the effect of liquid entrapment inside the crack is not seen in this study.

3.1 Implanting the initiating RCF crack

A 3D crack is implanted into the FE mesh with the geometry prescribed in Fig. 3. The front view of the crack plane in the FE model is shown in Fig. 5(a) with definitions of the crack mouth boundary and the crack tip curve. A numbering convention is proposed in this figure to address

the histories of stress intensity factors in the nodes of the crack tip. Based on this definition, nodes 1 and 41 are the boundaries of the crack tip at the rail surface and node 21 is the crack tip midpoint. Note that node 1 is located at the gauge corner side of the rail.

3.2 Calculation of SIFs

For isotropic materials, singular stresses and displacements near the crack tip can be described by SIFs (Zhu and Smith 1995). Various methods are available for calculating SIFs and crack tip singular stresses using FEM (Blackburn 1973, Anderson 2005). The displacement method based on FEM is used in the present research to calculate the SIFs of the crack tip. As shown in Fig. 5(b), a local coordinate system is defined for each singular node at the crack tip. Displacement histories of the nodes adjacent to the crack tip were used for SIF calculations. In this figure x, y and z are the axes of the local coordinate system, aligned toward the crack front with the origin at the crack tip. Using this method, a crack will experience three basic types of loading, i.e. opening mode, shearing mode and tearing mode.

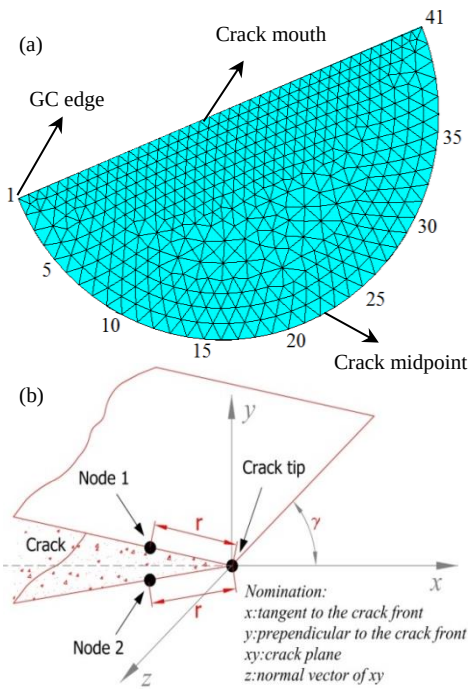

Fig. 5. (a) Definition of the discretised nodes and crack boundaries in the crack front, (b) local coordinate system of the nodes at the crack tip

The SIFs at the crack tip (Nodes 1 to 41) were calculated using nodal displacements of their adjacent nodes in the FE model. According to (Farjoo, Pal et al. 2012), SIFs are related to relative displacements of the associated nodes next to the crack tip in local axes:

$$K_I = \frac{E}{8(1-\upsilon^2)}\sqrt{\frac{2\pi}{r}}(y_1 - y_2) \quad (1)$$

$$K_{II} = \frac{E}{8(1-\upsilon^2)}\sqrt{\frac{2\pi}{r}}(x_1 - x_2) \quad (2)$$

$$K_{III} = \frac{E}{8(1-\upsilon^2)}\sqrt{\frac{2\pi}{r}}(z_1 - z_2) \quad (3)$$

where, K_I, K_{II}, K_{III} are the SIFs in opening, shearing and tearing modes; r is the distance of nodes from the crack front; x, y and z are the local displacements of the nodes in the crack front. xy us the crack plane with its normal vector z. In order to estimate the equivalent SIF of the rail nodes in the mixed-mode fatigue crack growth, the formula suggested in (Richard, Sander et al. 2008) was used. The equivalent SIF (K_{eq}) in this formula combines the effects of all fracture modes in the fatigue analysis:

$$K_{eq} = \frac{K_I}{2} + \frac{1}{2}\sqrt{K_I^2 + 4(1.155K_{II})^2 + 4K_{III}^2} \quad (4)$$

Table 2: Mechanical/loading parameters of the wheel-track system

Parameters	**Values**
Static wheel load, P_0 *(kN)*	120
Wheel weight *(kg)*	900
Sleeper mass M_s *(kg)*	280
Stiffness of ballast, K_b *(kN/m)*	45000
Damping of ballast, C_b *(N.s/m)*	32000
Stiffness of rail pad, K_p *(kN/m)*	1300000
Damping of rail pad, C_p *(N.s/m)*	45000
Stiffness of primary suspension, K_c *(kN/m)*	880
Damping of primary suspension, C_c *(N.s/m)*	4000
Young's modulus of wheel-rail, E_r *(GP)*	210
Poisson's ratio of wheel-rail material, v_r	0.3
Density of wheel-rail material, ρ_r *(kg/m3)*	7800
Young's modulus of concrete, E_c *(GP)*	38.4
Poisson's ratio of concrete material, v_c	0.2
Density of sleeper material, ρ_c *(kg/m3)*	2520
Rolling speed *(km/h)*	140
Friction coefficient between wheel and rail	0.6
Friction coefficient between the crack faces	0.05
Traction coefficient	0.25
Maximum calculated contact pressure*(MPa)*	1316

4 Results of SIF calculations

This section presents the results of SIF calculations of the nodes at the crack tip. One loading cycle of a wheel running over the cracked rail was simulated. A travelling time between -4b and 4b (b is the semi-major axis of the contact patch) was considered for calculating the SIFs. The SIFs obtained from the FE simulation are plotted in Fig. 6-8. The parameter x in these graphs is the distance of wheel centre from the crack mouth. Hence, a negative x represents the situation when the wheel is approaching to the crack mouth and a positive x is for the wheel when it has passed the crack. The value x=0 corresponds to the wheel position exactly on top of the crack mouth. For better illustration, SIFs of the negative wheel positions were plotted separately from the positive ones. The abscissas of these graphs represent the nodes of the crack tip curve shown in Fig. 5. The dimensionless SIF in Fig. 6-8 equals the original SIF divided by the maximum pressure, multiplied by the square root of the contact path semi-axis b.

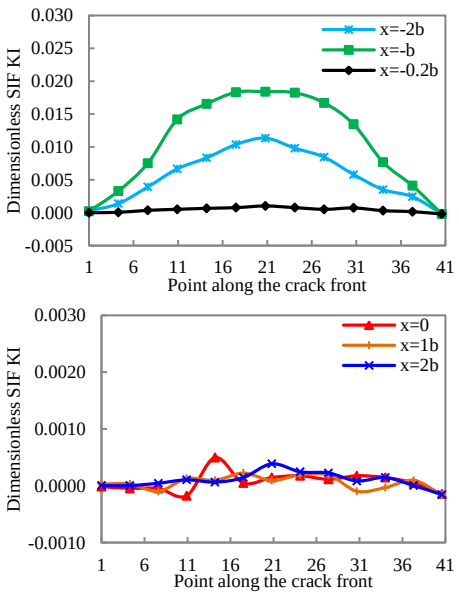

Fig. 6. The histories of K_I along the crack tip at three wheel locations (a) before reaching the crack mouth, (b) after passing the crack

5 Comparisons with a benchmark

In order to see the effectiveness of the proposed model, the SIFs obtained in the present study were compared with the Bogdanski's results (Bogdański and Lewicki 2008). This benchmark model uses a rail block with a flat surface laid on fixed boundary conditions. Detail of this model is described in (Bogdański and Lewicki 2008). The geometry of the crack and the loading conditions in the benchmark model were relatively different from the present work. The size of the crack (semi-elliptic exes) in the present study was relatively 40% smaller than that of the benchmark model to be more representative to the early life of the RCF crack.

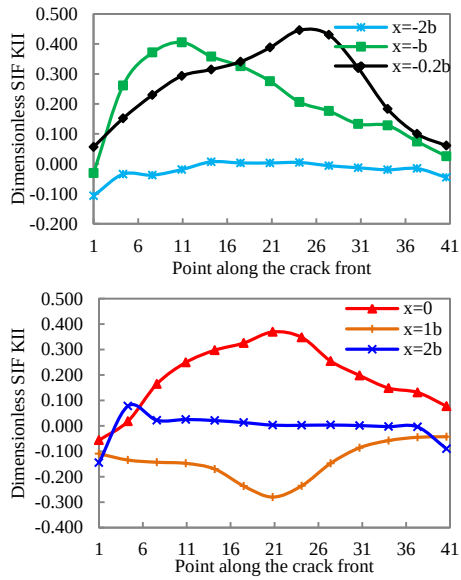

Fig. 7. The histories of K_{II} along the crack tip at three wheel locations (a) before reaching the crack mouth, (b) after passing the crack

The traction coefficient of the Bogdanski's model was -0.1 and the maximum contact pressure was p_0 = 740MPa. The same values are used in this section for the sake of comparison. The values of friction, crack size, contact patch size and material properties were also taken identical to (Bogdański and Lewicki 2008) and the SIFs were calculated again. The SIF distributions in the two models are plotted together in Fig. 9.

These results were obtained for two wheel positions, i.e. -0.8b and -0.2b; it is because only these results were available in the prescribed benchmark model. Note that the SIFs of the benchmark model were taken without the influence of water entrapment in crack propagation process.

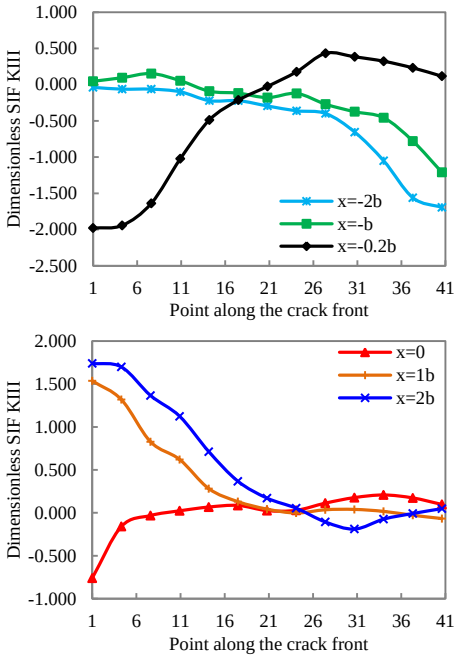

Fig. 8. The histories of K_{III} along the crack tip at three wheel locations (a) before reaching the crack mouth, (b) after passing the crack

Comparing these results, a number of observations were made:

1) The SIFs for all the fatigue propagation modes (mode I, II, III) were in good agreement with those of the Bogdanski's model. This was the case both wheel positions (-0.8b, -0.2b). Apart from negligible difference in peak quantities, good agreement was seen in SIF distributions (trends in different nodes) in the two models.

2) According to Fig. 9, both models led to higher opening and shearing SIFs in the crack midpoint (node 21) than the other nodes in the crack tip. This means K_I and K_{II} in the crack midpoint were more dominant than the other nodes. The SIFs of the crack edges (node 1, 41) were almost zero in the two models and in every wheel location.

3) From the data in figure 9(c), it is apparent that the crack midpoint relatively had zero K_{III} in both models.

In total, the SIF results were in good agreement with the benchmark model in terms of their general trend at different locations of the crack tip.

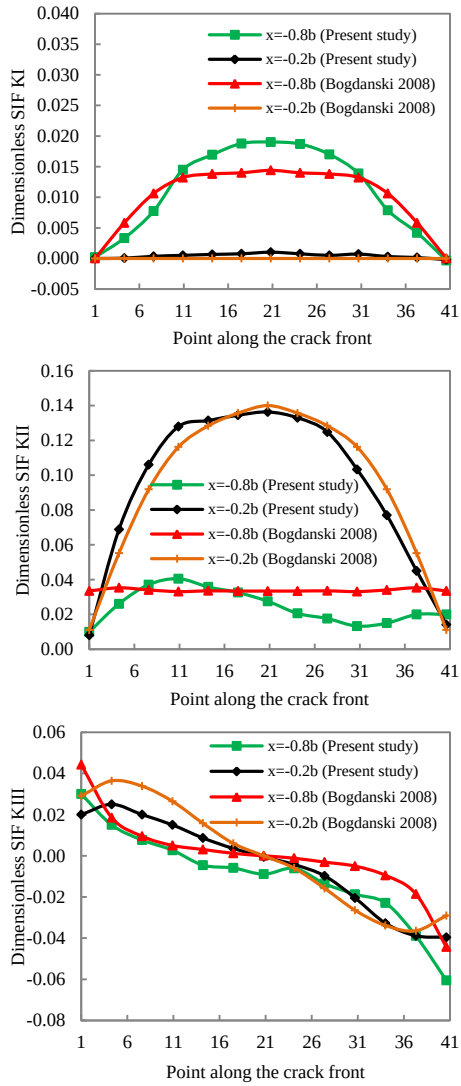

Fig. 9. Comparing the results of the FE simulations with the benchmark model, (a) distributions of K_I, (b) distributions of K_{II}, (c) distributions of K_{III}

5 Conclusions

This research calculated the stress intensity factors of an initiating RCF crack tip using a 3D model of the wheel-track system. The SIFs in the present research were compared with a benchmark model in the literature. According to the results, distributions of SIFs (for all the crack propagation modes I, II, III) were in good agreement with the benchmark model. In both

models, the opening and shearing modes of the crack midpoint were more significant than the other nodes in the crack tip. The crack midpoint relatively had zero K_{III} in both models. Taking these findings together, the two models showed a reasonable agreement on SIF trends in different nodes of the crack tip. However, the proposed model of the wheel-track system in the present research has the capability of considering dynamic impacts due to e.g. the presence of defects or irregularities in the modelling process. This will be a subject of further research on this topic.

Acknowledgment

This research is part of an ExploRail project namely as Development of High–Performance Rail through Intelligent Metallurgy and Engineering (PRIME), in Delft University of Technology. This project (Code: 11247/ C38A07) is funded by Dutch rail infra manager ProRail and the Netherlands organization for scientific research (STW/NWO).

References

Anderson, T. L. (2005). Fracture mechanics: fundamentals and applications, CRC press.

Blackburn, W. (1973). "Calculation of stress intensity factors at crack tips using special finite elements." The mathematics of finite elements and applications: 327-336.

Bogdański, S. (2005). "Predicting the growth of RCF crack with the use of the 3D multi size finite element model." Tribology and Interface Engineering Series **48**: 709-721.

Bogdański, S. and P. Lewicki (2008). "3D model of liquid entrapment mechanism for rolling contact fatigue cracks in rails." Wear **265**(9): 1356-1362.

Bogdanski, S., M. Olzak and J. Stupnicki (1998). "Numerical modelling of a 3D rail RCF 'squat'-type crack under operating load." Fatigue & Fracture of Engineering Materials & Structures **21**(8): 923-935.

Farjoo, M., S. Pal, W. Daniel and P. A. Meehan (2012). "Stress intensity factors around a 3D squat form crack and prediction of crack growth direction considering water entrapment and elastic foundation." Engineering Fracture Mechanics **94**: 37-55.

Kim, J. K. and C. S. Kim (2002). "Fatigue crack growth behavior of rail steel under mode I and mixed mode loadings." Materials Science and Engineering: A **338**(1): 191-201.

Naeimi, M., Z. Li and R. Dollevoet (2015). Nucleation of squat cracks in rail, calculation of crack initiation angles in three dimensions. Journal of Physics: Conference Series, IOP Publishing.

Pal, S., W. J. T. Daniel and M. Farjoo (2013). "Early stages of rail squat formation and the role of a white etching layer." International Journal of Fatigue **52**: 144-156.

Richard, H. A., M. Sander, M. Fulland and G. Kullmer (2008). "Development of fatigue crack growth in real structures." Engineering Fracture Mechanics **75**(3–4): 331-340.

Ringsberg, J. and B. Josefson (2001). "Finite element analyses of rolling contact fatigue crack initiation in railheads." Proceedings of the Institution of Mechanical Engineers, Part F: Journal of Rail and Rapid Transit **215**(4): 243-259.

Ringsberg, J., M. Loo-Morrey, B. Josefson, A. Kapoor and J. H. Beynon (2000). "Prediction of fatigue crack initiation for rolling contact fatigue." International Journal of Fatigue **22**(3): 205-215.

Ringsberg, J. W. and A. Bergkvist (2003). "On propagation of short rolling contact fatigue cracks." Fatigue & Fracture of Engineering Materials & Structures **26**(10): 969-983.

Simon, S., A. Saulot, C. Dayot, X. Quost and Y. Berthier (2013). "Tribological characterization of rail squat defects." Wear **297**(1-2): 926-942.

Zhao, X. and Z. Li (2011). "The solution of frictional wheel–rail rolling contact with a 3D transient finite element model: Validation and error analysis." Wear **271**(1–2): 444-452.

Zhao, X., Z. Li and R. Dollevoet (2013). "The vertical and the longitudinal dynamic responses of the vehicle–track system to squat-type short wavelength irregularity." Vehicle System Dynamics **51**(12): 1918-1937.

Zhao, X., Z. Li and R. Dollevoet (2014). "Influence of the fastening modeling on the vehicle-track interaction at singular rail surface defects." Journal of Computational and Nonlinear Dynamics.

Zhu, W. X. and D. J. Smith (1995). "On the use of displacement extrapolation to obtain crack tip singular stresses and stress intensity factors." Engineering Fracture Mechanics **51**(3): 391-400.